



1 **Significant wintertime PM<sub>2.5</sub> mitigation in the Yangtze**  
2 **River Delta, China from 2016 to 2019: observational**  
3 **constraints on anthropogenic emission controls**

4 Liqiang Wang<sup>1</sup>, Shaocai Yu<sup>\*,1,2</sup>, Pengfei Li<sup>\*,3,1</sup>, Xue Chen<sup>1</sup>, Zhen Li<sup>1</sup>, Yibo Zhang<sup>1</sup>,  
5 Mengying Li<sup>1</sup>, Khalid Mehmood<sup>1</sup>, Weiping Liu<sup>1</sup>, Tianfeng Chai<sup>4</sup>, Yannian Zhu<sup>5</sup>, Daniel  
6 Rosenfeld<sup>6</sup>, and John H. Seinfeld<sup>2</sup>

7  
8 <sup>1</sup>Research Center for Air Pollution and Health; Key Laboratory of Environmental  
9 Remediation and Ecological Health, Ministry of Education, College of Environment  
10 and Resource Sciences, Zhejiang University, Hangzhou, Zhejiang 310058, P.R. China

11 <sup>2</sup>Division of Chemistry and Chemical Engineering, California Institute of Technology,  
12 Pasadena, CA 91125, USA

13 <sup>3</sup>College of Science and Technology, Hebei Agricultural University, Baoding, Hebei  
14 071000, P.R. China

15 <sup>4</sup>Air Resources Laboratory, NOAA, Cooperative Institute for Satellite Earth System  
16 Studies (CISESS), University of Maryland, College Park, USA

17 <sup>5</sup>Meteorological Institute of Shanxi Province, 36 Beiguangzhengjie, Xi'an 710015,  
18 China

19 <sup>6</sup>Institute of Earth Science, The Hebrew University of Jerusalem, Jerusalem, Israel

20

21 Correspondence to:

22 Shaocai Yu (shaocaiyu@zju.edu.cn); Pengfei Li (lpf\_zju@163.com)

23

24

25

26

27

28

29

30

31



32 **ABSTRACT**

33 Ambient fine particulate matter (PM<sub>2.5</sub>) mitigation relies strongly on anthropogenic  
34 emission control measures, the actual effectiveness of which is challenging to pinpoint  
35 owing to the complex synergies between anthropogenic emissions and meteorology.  
36 Here, observational constraints on model simulations allow us to derive not only  
37 reliable PM<sub>2.5</sub> evolution but also accurate meteorological fields. In this study, we isolate  
38 meteorological factors to achieve reliable estimates of surface PM<sub>2.5</sub> responses to both  
39 long-term and emergency emission control measures from 2016 to 2019 over the  
40 Yangtze River Delta (YRD), China. The results show that long-term emission control  
41 strategies play a crucial role in curbing PM<sub>2.5</sub> levels (> 14 µg/m<sup>3</sup>, 19%), especially in  
42 the megacities and other areas with abundant anthropogenic emissions. The G20  
43 summit hosted in Hangzhou in 2016 provides a unique and ideal opportunity involving  
44 the most stringent, even unsustainable, emergency emission control measures. For the  
45 winter time periods from 2016 to 2019, the most substantial declines in PM<sub>2.5</sub>  
46 concentrations (~ 35 µg/m<sup>3</sup>, ~ 59%) are thus achieved in Hangzhou and its surrounding  
47 areas. The following hotspots also emerge in megacities, especially in Shanghai (32  
48 µg/m<sup>3</sup>, 51%), Nanjing (27 µg/m<sup>3</sup>, 55%), and Hefei (24 µg/m<sup>3</sup>, 44%). Compared to the  
49 long-term policies from 2016 to 2019, the emergency emission control measures  
50 implemented during the G20 Summit achieve more significant decreases in PM<sub>2.5</sub>  
51 concentrations (17 µg/m<sup>3</sup> and 41%) over most of the whole domain, especially in  
52 Hangzhou (24 µg/m<sup>3</sup>, 48%) and Shanghai (21 µg/m<sup>3</sup>, 45%). By extrapolation, we derive  
53 insight into the magnitude and spatial distributions of PM<sub>2.5</sub> mitigation potentials across  
54 the YRD, revealing significantly additional rooms for curbing PM<sub>2.5</sub> levels.

55 **1 INTRODUCTION**

56 Anthropogenic induced fine particulate matter (particulate matter with an aerodynamic  
57 diameter smaller than 2.5 µm, hereinafter denoted as PM<sub>2.5</sub>) is a principal object of air  
58 pollution control in China (Huang et al., 2014; Zhang et al., 2015). Moreover, the  
59 government has made major strides in curbing anthropogenic emissions (e.g., SO<sub>2</sub>, NO<sub>x</sub>,  
60 and CO) via both long-term and emergency measures during the past decade (Yan et  
61 al., 2018; Yang et al., 2019; Zhang et al., 2012). However, owing to the complex  
62 synergy of chemistry and meteorology (Seinfeld and Pandis, 2016), the extent to which  
63 these measures have abated PM<sub>2.5</sub> pollution, as well as the attainable mitigation



64 potential, remains unclear (An et al., 2019). The challenge involves reliably representing  
65 substantial and rapid changes in anthropogenic emissions resulting from both long-term  
66 and emergency control measures (Chan and Yao, 2008).

67 Since 2013, the China National Environmental Monitoring Center (CNEMC) has  
68 established 1415 ground-based  $PM_{2.5}$  measurement sites across 367 key cities (Zhang  
69 and Cao, 2015). In contrast to satellite observations with sparse spatiotemporal  
70 coverages (Ma et al., 2014, 2015; Xue et al., 2019), these ground sites can provide  
71 hourly  $PM_{2.5}$  concentrations at high spatial resolution in urban areas. Data assimilation  
72 (DA) methods that have been widely used in meteorology can be extended to integrate  
73 those continuous observational constraints with chemical transport models (CTMs)  
74 (Bocquet et al., 2015; Chai et al., 2017; Gao et al., 2017; Jung et al., 2019; Ma et al.,  
75 2019). It has been demonstrated that the capability of several representative DA  
76 methods, such as the optimal interpolation (OI) (Chai et al., 2017), 3D/4D variational  
77 methods (Li et al., 2016), and the ensemble Kalman filter algorithm (Chen et al., 2019a),  
78 can bridge the estimation gaps between observed and simulated results. Thus,  
79 observational constraints can be taken full advantage of to identify the effects of  
80 anthropogenic emission controls.

81 From the perspective of policymaking, 2016 was a special year for air pollution control  
82 in China. Since 2013, the Chinese government instituted extensive policies, such as the  
83 Air Pollution Prevention and Control Action Plan. These strategies were initiated and  
84 implemented through generally shutting down or relocating high emission traditional  
85 industrial enterprises (Sheehan et al., 2014; Shi et al., 2016; Xie et al., 2015). Starting  
86 from January 1, 2016, the relevant law, as well as the “Blue Sky Battle Plan”, came into  
87 full effect and profoundly shifted how China prioritized air quality management (Feng  
88 and Liao, 2016; Li et al., 2019c). Hence, we address the impact of long-term emission  
89 control strategies on  $PM_{2.5}$  mitigation from 2016 onward.

90 The G20 summit hosted in Hangzhou in 2016 (hereinafter termed the G20 summit)  
91 provides a unique and ideal opportunity to further explore the attainable  $PM_{2.5}$   
92 mitigation potential across the Yangtze River Delta (YRD) (Li et al., 2017b; Ma et al.,  
93 2019; Shu et al., 2019; Yang et al., 2019). Prior to and during this period, the Chinese  
94 government enforced historically strictest, even unsustainable, emergency emission  
95 control measures, including significant control, even cessation, of factory operations,  
96 restrictions on vehicles in the region, thus achieving unprecedented  $PM_{2.5}$  abatement at  
97 specific locations (e.g., Hangzhou) (Ji et al., 2018; Li et al., 2017b; Yang et al., 2019).



98 The role of these emergency emission control measures, that is, the relatively localized  
99 PM<sub>2.5</sub> mitigation potential, should thus be identified, and further extended to the entire  
100 YRD.

101 To quantify the effectiveness of the emission control strategies, we constrained a state-  
102 of-the-art CTM by a reliable DA method with extensive chemical and meteorological  
103 observations. This comprehensive technical design provides a crucial advance in  
104 isolating the influences of emission changes and meteorological perturbations over the  
105 YRD from 2016 to 2019, thus deriving unprecedented estimates of PM<sub>2.5</sub> responses to  
106 both long-term and emergency emission control measures, and establishing the first  
107 map of the PM<sub>2.5</sub> mitigation potential across the YRD.

## 108 **2 MATERIALS AND METHODS**

### 109 **2.1 The two-way coupled WRF-CMAQ model**

110 The two-way coupled Weather Research and Forecasting (WRF) and Community  
111 Multiscale Air Quality (CMAQ) model (the WRF-CMAQ model), as the key core of  
112 the DA system, was applied to investigate the ambient PM<sub>2.5</sub> feedbacks under different  
113 constraining circumstances (Byun and Schere, 2006; Wong et al., 2012; Yu et al., 2014).  
114 We utilized the CB05 and AERO6 modules for gas-phase chemistry and aerosol  
115 evolution (Carlton et al., 2010; Yarwood et al., 2005), respectively. Both secondary  
116 inorganic and organic aerosol (i.e., SIA and SOA) were thus explicitly treated with the  
117 AERO6 scheme in the WRF-CMAQ model. Together with the ISORROPIA II  
118 thermodynamic equilibrium module (Fountoukis and Nenes, 2007), SIA in the Aitken  
119 and accumulation modes (Binkowski and Roselle, 2003) was assumed to be in  
120 thermodynamic equilibrium with the gas phase, while that in the coarse mode was  
121 treated dynamically. SOA was formed via gas-, aqueous-, and aerosol-phase oxidation  
122 processes, such as in-cloud oxidation of glyoxal and methylglyoxal, absorptive  
123 partitioning of condensable oxidation of monoterpenes, long alkanes, low-yield  
124 aromatic products (based on m-xylene data), and high-yield aromatics, and NO<sub>x</sub>-  
125 dependent yields from aromatic compounds<sup>31</sup>. The subsequent reaction products can be  
126 divided into two groups: non-volatile semi-volatile (Carlton et al., 2010). Such  
127 treatments have been widely used and comprehensively validated. Longwave and  
128 shortwave radiation were both treated using the RRTMG radiation scheme (Clough et  
129 al., 2005). Related land surface energy balance and planetary boundary layer



130 simulations were included in the Pleim-Xiu land surface scheme (Xiu and Pleim, 2001)  
131 and the asymmetric convective model (Pleim, 2007b, 2007a), respectively. The two-  
132 moment Morrison cloud microphysics scheme (Morrison and Gettelman, 2008) and the  
133 Kain-Fritsch cumulus cloud scheme (Kain, 2004) were employed for simulating  
134 aerosol-cloud interactions and precipitation. Default settings in the model were used to  
135 prescribe chemical initial and boundary conditions. A spin-up period of seven days was  
136 carried out in advance to eliminate artefacts associated with initial conditions.  
137 Meteorological initial and boundary conditions were obtained from the ECMWF  
138 reanalysis dataset with the spatial resolution of  $1^\circ \times 1^\circ$  and temporal resolution of 6  
139 hours (<http://www.ecmwf.int/products/data>). Biogenic and dust emissions were  
140 calculated on-line using the Biogenic Emission Inventory System version 3.14  
141 (BEISv3.14) (Carlton and Baker, 2011) and a windblown dust scheme embedded in  
142 CMAQ (Choi and Fernando, 2008), respectively.

143 The horizontal domain of the model covered mainland China by a  $395 \times 345$  grid with  
144 a 12 km horizontal resolution following a Lambert Conformal Conic projection (Figure  
145 1). In terms of the vertical configuration, 29 sigma-pressure layers ranged from the  
146 surface to the upper level pressure of 100 hPa, 20 layers of which are located below  
147 around 3 km to derive finer meteorological and chemical characteristics within the  
148 planetary boundary layer.

149 As a state-of-the-art CTM, the WRF-CMAQ model has been widely used to simulate  
150 spatiotemporal  $PM_{2.5}$  distributions at regional scales. However, model biases remain,  
151 mainly due to imperfect representations of chemical and meteorological processes.  
152 Inaccurate anthropogenic emissions will exacerbate these biases. Therefore, external  
153 constraints on simulated results enforced by the DA method will be taken into account  
154 in order to optimize spatiotemporal  $PM_{2.5}$  distributions (Bocquet et al., 2015).

## 155 **2.2 Prior anthropogenic emissions**

156 The prior anthropogenic emissions were obtained from the Multi-resolution Emission  
157 Inventory for China version 1.2 (MEIC) (Li et al., 2017a), which contained primary  
158 species (e.g., primary  $PM_{2.5}$ ,  $SO_2$ ,  $NO_x$ , CO, and  $NH_4$ ) from five anthropogenic sectors  
159 (i.e., agriculture, power plant, industry, residential, and transportation). This inventory  
160 was initially designed with the spatial resolution of  $0.25^\circ \times 0.25^\circ$  and thus needed to be  
161 reallocated to match the domain configuration (i.e.,  $12\text{km} \times 12\text{km}$ ) in the study.  
162 Recent findings show that MEIC generally provides reasonable estimates of total



163 anthropogenic emissions for several typical regions in China, such as the Beijing-  
164 Tianjin-Hebei region, the YRD, and the Pearl River Delta region (Li et al., 2017a).  
165 Nevertheless, large uncertainties in spatial proxies (e.g., population density and road  
166 networks) still exist within these specific regions (Geng et al., 2017). More, MEIC was  
167 originally constructed for the 2016 base year. Hence, owing to the impact of the long-  
168 term emission control measures, MEIC was considered to be inappropriate for this  
169 study period (i.e., 2019). Comparatively, emergency control measures could give rise  
170 to much more significant emission controls in the short term, thereby leading to further  
171 uncertainties.

### 172 **2.3 Observational network**

173 To track real-time air quality in China, the National Environmental Monitoring Center  
174 (CNEMC, <http://www.cnemc.cn/>) has established 1415 sites across 367 cities since  
175 2013 (Figure 1). Among these, 244 monitoring sites were densely distributed in 6660  
176 grids across the YRD providing hourly PM<sub>2.5</sub> measurements, resulting in potential  
177 excellent roles in constraining simulated PM<sub>2.5</sub> (Bocquet et al., 2015). In this study, we  
178 applied observed PM<sub>2.5</sub> concentrations to constrain and evaluate the model performance.  
179 It is worth noting that the constraining capability of those observations varies depending  
180 on specific configurations (e.g., the nature of the utilized DA method, the assimilation  
181 frequency, and the representative errors of observations) (Bocquet et al., 2015; Chai et  
182 al., 2017; Ma et al., 2019; Rutherford, 1972). Therefore, we employed all available  
183 hourly observations along with the specific DA method to maximize the model  
184 performance in simulating the spatiotemporal patterns of PM<sub>2.5</sub>. In turn, the  
185 corresponding results need to be further assessed against available observations.

### 186 **2.4 Optimal interpolation**

187 Optimal interpolation (OI) was chosen to assimilate hourly observations into the WRF-  
188 CMAQ model, aiming to generate the accurate state of spatiotemporal PM<sub>2.5</sub>  
189 distributions. Compared to the solely model-dependent results, this constraining  
190 method relies on observations and thus makes it possible to minimize model  
191 uncertainties in optimizing the spatiotemporal PM<sub>2.5</sub> changes resulting from emission  
192 controls (Chai et al., 2017; Jung et al., 2019). The analysed states from the OI method  
193 were calculated based on the following interpolation equation:

$$194 \quad \mathbf{X}^a = \mathbf{X}^b + \mathbf{B}\mathbf{H}^T(\mathbf{H}\mathbf{B}\mathbf{H}^T + \mathbf{O})^{-1}(\mathbf{Y} - \mathbf{H}\mathbf{X}^b) \quad (1)$$



195 where  $\mathbf{X}^a$  and  $\mathbf{X}^b$  denote the constrained and background (simulated) values,  
196 respectively.  $\mathbf{B}$  and  $\mathbf{O}$  are background and observation error-covariance matrices,  
197 respectively, for which we assumed no correlation in this study.  $\mathbf{H}$  refers to a linearized  
198 observational operator, and  $\mathbf{Y}$  represents the observation vector. The OI method is  
199 described in detail in Adhikary et al. (2008).

200 Once available measurements were assimilated, the states of the simulated variables  
201 were adjusted from their background values to corresponding analysis states using the  
202 scaling ratio  $X^a/X^b$  obtained following equation (1). As the measurements were  
203 conducted at the surface, this ratio at each grid cell was used to scale all aerosol  
204 components below the boundary layer top. Such simplification compensated for the  
205 lack of information to constrain speciated aerosol components or their vertical  
206 distributions.

207 It is crucial to identify the background error covariance matrix  $\mathbf{B}$ , since it determines  
208 the corrections to be applied to the background fields in order to better match the data.  
209 First, we applied the Hollingsworth-Lönnerberg method within the YRD to establish the  
210 correlation coefficients (averaged over 10 km bins) with the separation distances (Chai  
211 et al., 2017; Hollingsworth and Lönnerberg, 1986). Figure 2 shows that the separation  
212 distance of  $\sim 180$  km could be treated as the threshold pinpointing the key value of the  
213 correlation coefficients ( $e^{-1}$ ). In this study, observations beyond the background-error  
214 correlation length scale would have no effect on  $X^a$ . Following Chai et al. (Chai et al.,  
215 2017), the standard deviation of the background errors was assigned as 60% of the  
216 background values, while the observational errors were assumed to be  $\pm 20\%$  of the  
217 measurement values. Despite the stationary background error correlation coefficients,  
218 the dynamic standard deviations of the background errors would still lead the  
219 background error covariance to be inhomogeneous.

## 220 2.4 Experiment design

221 Anthropogenic emission controls and meteorological perturbations are both critical  
222 factors that dominate interannual and daily variations in ambient  $\text{PM}_{2.5}$  (Zhang et al.,  
223 2019). Our major objective is to isolate the impacts of emission-oriented long-term and  
224 emergency measures and further explore the attainable  $\text{PM}_{2.5}$  mitigation potential. We  
225 designed three sets of experiments, which focused on three time periods, January 2016,



226 January 2019, and the G20 period (from August 26, 2016 to September 7, 2016),  
227 respectively (Table 1).

228 For all experiments, the prior anthropogenic emissions were kept consistent (i.e.,  
229 MEIC), while the ECMWF reanalysis datasets accounted for the hourly observational  
230 constraints on spatiotemporal meteorological evolutions. These configurations both  
231 unify the chemical inputs for the WRF-CMAQ model and derive reliable  
232 meteorological fields. Hence, the extent to which we introduce observational  
233 constraints on simulated PM<sub>2.5</sub> variations using the OI method is the key to isolate the  
234 impacts of anthropogenic emission controls.

235 Specifically, the differences in the constrained PM<sub>2.5</sub> concentrations between DA\_2016  
236 and DA\_2019 reflected the net effects of anthropogenic emission controls and  
237 meteorological perturbations between 2016 and 2019. By separating the impacts of the  
238 latter, that is, the discrepancies in simulated PM<sub>2.5</sub> concentrations between NO\_2016  
239 and NO\_2019, we can isolate the effects of anthropogenic emission controls  
240 attributable to long-term strategies (Chen et al., 2019a).

241 The G20 summit provided a unique opportunity to realize the PM<sub>2.5</sub> mitigation potential  
242 in specific regions (Li et al., 2019a, 2017b; Ma et al., 2019; Shu et al., 2019; Yang et al.,  
243 2019). This is due to the fact that the Chinese government implemented the most  
244 historically stringent, even unsustainable, strategies to curb anthropogenic emissions  
245 during that period in Hangzhou and surrounding areas. To quantify the projected PM<sub>2.5</sub>  
246 abatement, we adopted the abovementioned method to constrain the unique PM<sub>2.5</sub>  
247 variations in the DA\_G20 experiment and further compared the corresponding results  
248 with those of the sole model-dependent analysis (i.e., NO\_G20). However, the  
249 subsequent discrepancies were related not only to the effects of emergency  
250 anthropogenic emission strategies but also to the inherent biases mainly due to the prior  
251 emission inventory (Zhang et al., 2019). In theory, such biases would generally remain  
252 unchanged in the short term when no emergency emission controls occurred. Their  
253 consequent impacts could thus be stable under similar meteorological conditions.  
254 Therefore, to avoid additional uncertainties, the adjacent periods of the G20 summit  
255 (i.e., pre- and post- periods, from August 11 to August 23, 2016 and from September  
256 18 to September 30, 2016, respectively) are the optimal alternative to eliminate the  
257 impacts of those inherent biases. Figure S1 demonstrates the significantly similar  
258 meteorological fields among these three periods. As a result, the corresponding  
259 experiments (i.e., DA\_CON\_G20 and NO\_CON\_G20) (Table 1) were conducted. By



260 subtracting such differences, we could isolate the  $PM_{2.5}$  responses to the solely  
261 emergency anthropogenic emission strategies and finally achieve the  $PM_{2.5}$  mitigation  
262 potential for specific locations. Such localized  $PM_{2.5}$  mitigation potential should be  
263 further expanded to the entire YRD based on the impacts of both long-term and  
264 emergency strategies.

265 There is an essential prerequisite to above analysis. As the evaluation protocols, we  
266 need to verify that the DA experiments (i.e., DA\_2016, DA\_2019, DA\_G20, and  
267 DA\_CON\_G20) can reproduce the spatiotemporal variations in the  $PM_{2.5}$  and major  
268 meteorological fields (i.e., temperature, relative humidity, wind speed and air pressure)  
269 (Chai et al., 2017). Although SIA and SOA are key components of the ambient  $PM_{2.5}$ ,  
270 extensive measurements at the regional scale of these components are generally lacking.  
271 It is thus difficult to generate appropriate constraints on SIA and SOA (Chai et al., 2017;  
272 Gao et al., 2017). Note that different anthropogenic emissions might lead to inconsistent  
273 estimation of meteorological effects on ambient  $PM_{2.5}$  (Chen et al., 2019a, 2019b; Ma  
274 et al., 2019). To eliminate this doubt, we conducted sensitivity tests by reducing MEIC  
275 with three reasonable ratios (i.e., -5%, -25%, and -40%) over the YRD based on  
276 NO\_2016 and NO\_2019.

## 277 **3 RESULTS**

### 278 **3.1 Data assimilation performance**

279 Figure 3 shows spatial comparisons of hourly averaged concentrations of constrained  
280 and simulated  $PM_{2.5}$  (i.e., the ones from the cases with and without DA, respectively)  
281 with ground-level observations across the YRD for January 2016, January 2019, and  
282 the G20 summit. In the NO\_2016, NO\_2019, and NO\_G20 experiments, the simulated  
283  $PM_{2.5}$  concentrations generally overestimated observed values by 16 ~ 57  $\mu\text{g}/\text{m}^3$ ,  
284 especially those in Hangzhou and surrounding areas during the G20 summit ( $> 21$   
285  $\mu\text{g}/\text{m}^3$ ). Such prevailing overestimates were mainly a result of the prior anthropogenic  
286 emission inventory (i.e., MEIC), as a bottom-up product, which notably cannot capture  
287 interannual emission changes since the base year 2012, as well as the large emission  
288 controls resulting from the emergency controls during the G20 summit. By comparison,  
289 the constrained results significantly approach observations. Specifically, in the  
290 DA\_2016, DA\_2019, and DA\_G20 cases, the biases of the assimilated  $PM_{2.5}$  were all  
291 constrained in an extremely narrow range (i.e., 10  $\mu\text{g}/\text{m}^3$ , 12  $\mu\text{g}/\text{m}^3$ , and 13  $\mu\text{g}/\text{m}^3$ ,



292 respectively), suggesting that the DA method can reproduce the spatiotemporal  
293 distributions of surface  $PM_{2.5}$  at the regional scale.  
294 To achieve more targeted evaluations, it is necessary to further assess the ability of the  
295 DA method in reproducing the city-level  $PM_{2.5}$  responses. With the analysis of time  
296 series over the same periods, Figure 4 illustrates the comparisons between hourly  
297 observed, simulated, and constrained  $PM_{2.5}$  concentrations over the whole domain and  
298 four representative cities (i.e., Shanghai, Hangzhou, Nanjing, and Hefei). Similar to the  
299 spatial comparisons, the constrained  $PM_{2.5}$  generally reproduces the temporal variations  
300 in observations, while the model-dependent simulated results are prone to  
301 overestimating those observations, in particular, the peaks by  $85 \sim 257 \mu\text{g}/\text{m}^3$ .  
302 As expected, basic evaluation indicators (i.e., the NMB and R values) (Yu et al., 2006)  
303 of assimilated  $PM_{2.5}$  exhibited significantly better behaviour than those without  
304 constraints (Figure S2). Taking the simulated and assimilated results for Hangzhou  
305 during January 2016 as an example, the corresponding R values improved from 0.63 to  
306 0.98, while the NMB values were reduced from 17% to 3%. Similar improvements, but  
307 with varying extent, were found in other paired experiments. In addition, it should be  
308 emphasized that the differences between hourly constrained and simulated  $PM_{2.5}$   
309 concentrations for the year 2016 were almost lower than those for the year 2019,  
310 indicating the critical role of interannual continuous efforts on curbing anthropogenic  
311 emissions across the YRD.  
312 Owing to the fact that the distinct  $PM_{2.5}$  levels might also play a potential role in the  
313 DA performance, we thus separated the entire range of the observed  $PM_{2.5}$   
314 concentrations into four intervals (i.e.,  $< 35 \mu\text{g}/\text{m}^3$ ,  $35 \sim 75 \mu\text{g}/\text{m}^3$ ,  $75 \sim 115 \mu\text{g}/\text{m}^3$ , and  $>$   
315  $115 \mu\text{g}/\text{m}^3$ ), exactly corresponding to the continuously increasing  $PM_{2.5}$  levels. Figure  
316 S3 demonstrates that, relative to the sole model-dependent configurations, this  
317 constraining method could substantially strengthen the model performance, especially  
318 for the relatively elevated concentration intervals. Overall, the ranges of the NMB  
319 values and associated standard deviations decreased from  $-24 \sim 86\%$  to  $-9 \sim 25\%$  and  
320  $34 \sim 174 \mu\text{g}/\text{m}^3$  to  $12 \sim 52 \mu\text{g}/\text{m}^3$ , respectively. Theoretically, more frequent DA should  
321 lead to more robust simulations. Hourly observational constraints on the  $PM_{2.5}$   
322 concentrations were thus adopted to tackle this issue. This is the reason why the  
323 corresponding NMB values in the constraining cases roughly maintain stability,  
324 fluctuating over a narrow range (i.e.,  $\pm 20\%$ ) in the study periods (Figure S4). In



325 addition, given that the assimilated ERA reanalysis dataset has much wider spatial  
326 coverage than ground-based measurements, we also reproduced the spatiotemporal  
327 variations in the meteorological factors (e.g., temperature, relative humidity, wind  
328 speed, and air pressure) (Figures S5 ~ S8). Through the comprehensive evaluation  
329 statistics as summarized in Tables S1-S5, it has been demonstrated that the DA method  
330 can enable one to derive not only reliable  $PM_{2.5}$  evolution but also accurate  
331 meteorological fields.

### 332 **3.2 Ambient $PM_{2.5}$ responses to the long-term strategies**

333 The Chinese government has been implementing stringent emission control strategies  
334 since 2016, especially in the YRD (Feng and Liao, 2016; Li et al., 2019c). To quantify  
335 subsequent  $PM_{2.5}$  responses is thus the prerequisite to our final objective, that is, to  
336 explore the associated  $PM_{2.5}$  mitigation potential.

337 Interannual changes in spatiotemporal  $PM_{2.5}$  distributions depended strongly on both  
338 anthropogenic emission controls and meteorological variations from 2016 to 2019.  
339 Their combined effects were reflected by the differences between the constrained  
340 results from DA\_2016 and DA\_2019. As shown in Figure 5a, such net impacts led to  
341 prevailing  $PM_{2.5}$  abatement in the domain, especially in megacities, such as Shanghai  
342 ( $13 \mu\text{g}/\text{m}^3$ , 21%), Hangzhou ( $13 \mu\text{g}/\text{m}^3$ , 17%), Nanjing ( $6 \mu\text{g}/\text{m}^3$ , 8%), and Hefei ( $2$   
343  $\mu\text{g}/\text{m}^3$ , 2%). In addition, noticeable  $PM_{2.5}$  controls also occurred in the western and  
344 northern YRD, where abundant anthropogenic emissions are concentrated (Figure S9).  
345 Detailed differences are shown in Table S6.

346 Figure 5b highlights that the sole meteorological interferences played an extensively  
347 positive role in increasing the regional  $PM_{2.5}$  concentrations for most areas of the  
348 domain ( $\sim 12 \mu\text{g}/\text{m}^3$ , 15%). This also indirectly implied the importance of assimilating  
349 meteorology. Previous studies generally neglected the possibility that the large  
350 uncertainties in the prior anthropogenic emissions might transfer to the estimates of  
351 meteorological influences in turn (Chen et al., 2019b, 2019a). In this study, we have  
352 eliminated this speculation. As shown in Figure S10, even with the largest adjustment  
353 (i.e., -40%), such interferences could be well controlled within the 5% scope, let alone  
354 other tests (i.e., < 3%). Moreover, these findings are consistent with previous analyses  
355 (Cheng et al., 2019; Zhang et al., 2019), which generally reveal that, under the same  
356 meteorological condition, reasonable changes in the bottom-up emissions during a few  
357 years would not remarkably alter the meteorological effects on regional ambient  $PM_{2.5}$



358 (< 5%). As a result, some past studies even directly ignored such sensitivity tests  
359 without any discussion (Chen et al., 2019a). Therefore, by subtracting those  
360 meteorological influences from the combined outcomes, we can finally derive the  
361 contributions of anthropogenic emission controls to the PM<sub>2.5</sub> mitigation at the regional  
362 scale. Figure 5c illustrates that long-term emission control strategies from 2016 to 2019  
363 produced substantial (> 14 µg/m<sup>3</sup>, 19%) decreases in regional PM<sub>2.5</sub> concentrations,  
364 which are similar to those combined effects in terms of the spatial distributions.  
365 For the entire domain, as well as the four representative cities, the synergy between  
366 anthropogenic emission controls and meteorological interferences on the PM<sub>2.5</sub>  
367 concentrations were calculated at the city level (Figure 6). We found that their net  
368 effects resulted in uniformly positive mitigations as follows: -2 µg/m<sup>3</sup> (-3%), -13 µg/m<sup>3</sup>  
369 (-21%), -12 µg/m<sup>3</sup> (-17%), -6 µg/m<sup>3</sup> (-8%), and -2 µg/m<sup>3</sup> (-3%) for the whole domain,  
370 Shanghai, Hangzhou, Nanjing, and Hefei, respectively, while the concurrent  
371 meteorology offset such effects to different extents (5 ~ 18 µg/m<sup>3</sup>, 16 ~ 24%).  
372 The above findings confirmed that the PM<sub>2.5</sub> mitigation was dominated by  
373 anthropogenic emission controls, rather than meteorological variations. Furthermore,  
374 the corresponding spatiotemporal patterns were highly correlated to those of the prior  
375 anthropogenic emissions (Figure S9). This indicates that the long-term strategies are  
376 generally emission-oriented.

### 377 **3.3 Ambient PM<sub>2.5</sub> mitigation potential**

378 The G20 summit offered a unique and ideal opportunity to clarify the effects of the  
379 most stringent emission control measures across the YRD from 2016 to 2019, which  
380 could be regarded as the localized PM<sub>2.5</sub> mitigation potential. Figure 7a shows the  
381 spatial differences between the constrained and simulated PM<sub>2.5</sub> concentrations, which  
382 were extracted from DA\_G20 and NO\_G20, for the period of the G20 summit. Inherent  
383 biases remained, primarily attributable to the priori anthropogenic emissions. Their  
384 subsequent impacts were then quantified by comparing the discrepancies between the  
385 results from two additional experiments (i.e., DA\_CON\_G20 and NO\_CON\_G20)  
386 (Figure 7b). More, such impacts were associated with relatively low standard deviations  
387 (< 5%), thus presenting a stably spatiotemporal state (Figure S11). This means that such  
388 estimations were also suitable for the G20 summit. Therefore, by subtracting them, the  
389 re-corrected differences would reflect the actual effects of the most stringent emission  
390 control measures for the G20 summit (Figure 7c). Such hotspots with extremely



391 negative values reveal the dramatic  $PM_{2.5}$  mitigations for these specific locations. The  
392 corresponding largest decreases in  $PM_{2.5}$  concentrations ( $35 \mu\text{g}/\text{m}^3$ , 59%) occurred in  
393 Hangzhou and its surrounding areas, as expected. Following Hangzhou, other hotspots  
394 with relatively prominent declines also emerged in megacities, especially in Shanghai  
395 ( $32 \mu\text{g}/\text{m}^3$ , 51%), Nanjing ( $27 \mu\text{g}/\text{m}^3$ , 55%) and Hefei ( $24 \mu\text{g}/\text{m}^3$ , 44%). This behaviour  
396 could be explained by two inferences that: (i) local emission controls in Hangzhou were  
397 projected to be conducted with the maximum execution efficiency compared to those  
398 in surrounding regions; (ii) most of the emergency measurements generally targeted the  
399 vehicle and industry emissions that are clustered around the urban rather than rural areas.  
400 Compared to the long-term policies from 2016 to 2019, the emergency emission control  
401 measures implemented during the G20 Summit achieved more significant decreases in  
402  $PM_{2.5}$  concentrations ( $17 \mu\text{g}/\text{m}^3$  and 41%) over most of the whole domain, especially in  
403 Hangzhou ( $24 \mu\text{g}/\text{m}^3$ , 48%) and Shanghai ( $21 \mu\text{g}/\text{m}^3$ , 45%) (Figure 8). Detailed  
404 differences are summarized in Table S6.

405 To gain the regional  $PM_{2.5}$  mitigation potential, (i) we first pinpointed the main urban  
406 areas of Hangzhou that covered 25 grid cells (Figure S12), in which the most substantial  
407  $PM_{2.5}$  abatement, i.e., the localized  $PM_{2.5}$  mitigation potential ( $> 22 \mu\text{g}/\text{m}^3$  and  $> 59\%$ )  
408 were identified. (ii) As the above hypothesis, the spatial distributions of the regional  
409  $PM_{2.5}$  mitigation potential across the YRD were then assumed to follow those of the  
410 long-term strategy effects. (iii) Thus, by extrapolation in equal proportion following  
411 such patterns and the localized  $PM_{2.5}$  mitigation potential, we established the  
412 unprecedented map of the  $PM_{2.5}$  mitigation potential across the YRD (Figure 9a). It  
413 should be noted that, as long as three premises, including typical weather backgrounds,  
414 stable supply-side structures, and analogous emission control measures, remain  
415 unchanged, Figure 9a is a reliably quantitative reference to characterize the attainable  
416  $PM_{2.5}$  abatement for the YRD in future.

#### 417 **4 DISCUSSION**

418 The actual effectiveness of anthropogenic emission control measures, especially those  
419 directed at  $PM_{2.5}$  mitigation, has long been excluded from evaluation of air pollution  
420 policies in China, in part due to the complex synergy between anthropogenic emissions  
421 and meteorology. Here, we provide a novel approach to explore the  $PM_{2.5}$  responses to  
422 anthropogenic emission control measures and their mitigation potential from 2016 to  
423 2019 across the YRD, China. With the data assimilation method, these estimates are



424 projected to be highly reliable due to the sufficient observational constraints. The results  
425 demonstrate that long-term anthropogenic emission control strategies from 2016 to  
426 2019 have led to extensive impacts on PM<sub>2.5</sub> abatement across the YRD, especially in  
427 the megacities, Shanghai, Hangzhou, Nanjing, and Hefei. In the context of the G20  
428 summit, the emergency strategies could achieve significant PM<sub>2.5</sub> abatement (> 50%)  
429 at specific locations, (i.e., urban Hangzhou), representing the localized mitigation  
430 potential. By extrapolation based on the above results, we have established the first map  
431 of the PM<sub>2.5</sub> mitigation potential for the YRD.

432 Numerous analyses have focused on Hangzhou during the G20 summit to detect  
433 impacts of emergency emission controls (Li et al., 2019b, 2017b; Yu et al., 2018).  
434 However, previous analyses generally found more effective predictions (> 50%) at the  
435 city level. This discrepancy might be related to the fact that such results were generally  
436 based on sole model-dependent predictions, which are normally driven by uncertain  
437 bottom-up estimates of prior anthropogenic emissions. In addition, this study addresses  
438 the YRD after 2016. Besides, similar opportunities also occurred at other  
439 spatiotemporal scales, such as the “APEC Blue” in 2014 and “Parade Blue” in 2015  
440 over the Beijing-Tianjin-Hebei region (BTH) (Liu et al., 2016; Sun et al., 2016; Zhang  
441 et al., 2016). More aggressive achievements (> 55%) were generally attributed to  
442 emergency anthropogenic emission control measures (Sun et al., 2016). This might be  
443 related to the fact that, compared to the YRD, the BTH is associated with more  
444 rudimentary and abundant primary emissions (Zhang et al., 2019). The impacts of  
445 natural sources (e.g., biogenic emissions, wild fires, and natural dust) are not considered  
446 in this study. This is mainly because of two reasons. First, it has been widely  
447 demonstrated that biogenic emission changes are dominated by meteorological  
448 variations over a period of a few years (Wang et al., 2019). Moreover, the former is  
449 generally of minor significance for interannual PM<sub>2.5</sub> variations (Mu and Liao, 2014;  
450 Tai et al., 2012). Second, satellite products, including MOD14 and  
451 AIRIBQAP\_NRT.005 (<https://worldview.earthdata.nasa.gov/>), show that there was no  
452 noticeable wild fires and natural dust storms during this study period, thus allowing us  
453 to ignore the corresponding interferences.

454 This study takes the advantage of observational constraints to gain the regional PM<sub>2.5</sub>  
455 mitigation potential. It could be further optimized by more extensive observations.  
456 Besides, extending the PM<sub>2.5</sub> mitigation potential in urban Hangzhou during the study  
457 period to the entire YRD in other time periods may introduce some uncertainties. As



458 abovementioned, impacts of the extreme emergency emission controls are spatially  
459 inconsistent across the YRD. To explore regional PM<sub>2.5</sub> mitigation potential, it is thus  
460 unavoidable to extrapolate from local to regional scale. The consequent uncertainty  
461 mainly relates to the hypothesis that the spatial patterns of the PM<sub>2.5</sub> mitigation potential  
462 across the YRD should follow those of the impacts of the long-term emission control  
463 strategies. In addition, there are distinct DA methods (Bocquet et al., 2015). It is thus  
464 believed that replacing the OI with another DA algorithm would lead to slightly  
465 different results. Looking forward, continued advances in observational techniques,  
466 better understanding of chemical and meteorological processes, and their improved  
467 representations in CTMs are all factors that are critical to optimizing the estimates of  
468 the PM<sub>2.5</sub> mitigation potential.

#### 469 **ASSOCIATED CONTENT**

##### 470 **Supporting Information.**

471 Meteorological factors during the G20 summit and its adjacent periods (Figure S1).  
472 Model evaluation of the hourly simulated and constrained PM<sub>2.5</sub> as well as main  
473 meteorological factors (Figures S2 ~ S8); Prior anthropogenic emissions (Figure S9);  
474 Impacts of different emissions on the meteorology (Figure S10); Impacts of different  
475 emissions on the meteorology (Figure S11); The enlarged part in Figure 7c (Figure S12).

#### 476 **NOTES**

477 The authors declare no competing financial interest.

#### 478 **ACKNOWLEDGEMENTS**

479 This study was supported by the Department of Science and Technology of China (No.  
480 2016YFC0202702, 2018YFC0213506 and 2018YFC0213503), National Research  
481 Program for Key Issues in Air Pollution Control in China (No. DQGG0107) and  
482 National Natural Science Foundation of China (No. 21577126 and 41561144004).  
483 Pengfei Li is supported by Initiation Fund for Introducing Talents of Hebei Agricultural  
484 University (412201904).

#### 485 **REFERENCES**

486 Adhikary, B., Kulkarni, S., Dallura, A., Tang, Y., Chai, T., Leung, L. R., Qian, Y.,  
487 Chung, C. E., Ramanathan, V. and Carmichael, G. R.: A regional scale chemical



488 transport modeling of Asian aerosols with data assimilation of AOD observations  
489 using optimal interpolation technique, *Atmos Environ*, 42(37), 8600–8615, 2008.

490 An, Z., Huang, R.-J., Zhang, R., Tie, X., Li, G., Cao, J., Zhou, W., Shi, Z., Han, Y.,  
491 Gu, Z. and others: Severe haze in Northern China: A synergy of anthropogenic  
492 emissions and atmospheric processes, *Proc Natl Acad Sci*, 116(18), 8657–8666, 2019.

493 Binkowski, F. S. and Roselle, S. J.: Models-3 Community Multiscale Air Quality  
494 (CMAQ) model aerosol component 1. Model description, *J Geophys Res Atmos*,  
495 108(D6), 2003.

496 Bocquet, M., Elbern, H., Eskes, H., Hirtl, M., Žabkar, R., Carmichael, G. R.,  
497 Flemming, J., Inness, A., Pagowski, M., Pérez Camarero, J. L. and others: Data  
498 assimilation in atmospheric chemistry models: current status and future prospects for  
499 coupled chemistry meteorology models, *Atmos Chem Phys*, 15(10), 5325–5358,  
500 2015.

501 Byun, D. and Schere, K. L.: Review of the governing equations, computational  
502 algorithms, and other components of the Models-3 Community Multiscale Air Quality  
503 (CMAQ) modeling system, *Appl Mech Rev*, 59(2), 51–77, 2006.

504 Carlton, A. G. and Baker, K. R.: Photochemical modeling of the Ozark isoprene  
505 volcano: MEGAN, BEIS, and their impacts on air quality predictions, *Environ Sci  
506 Technol*, 45(10), 4438–4445, 2011.

507 Carlton, A. G., Bhave, P. V., Napelenok, S. L., Edney, E. O., Sarwar, G., Pinder, R.  
508 W., Pouliot, G. A. and Houyoux, M.: Model representation of secondary organic  
509 aerosol in CMAQv4. 7, *Environ Sci Technol*, 44(22), 8553–8560, 2010.

510 Chai, T., Kim, H.-C., Pan, L., Lee, P. and Tong, D.: Impact of Moderate Resolution  
511 Imaging Spectroradiometer Aerosol Optical Depth and AirNow PM<sub>2.5</sub> assimilation on  
512 Community Multi-scale Air Quality aerosol predictions over the contiguous United  
513 States, *J Geophys Res Atmos*, 122(10), 5399–5415, 2017.

514 Chan, C. K. and Yao, X.: Air pollution in megacities in China, *Atmos Environ*, 42(1),  
515 1–42, 2008.

516 Chen, D., Liu, Z., Ban, J., Zhao, P. and Chen, M.: Retrospective analysis of 2015-  
517 2017 wintertime PM<sub>2.5</sub> in China: response to emission regulations and the role of  
518 meteorology, *Atmos Chem Phys*, 19(11), 7409–7427, 2019a.

519 Chen, D., Liu, Z., Ban, J. and Chen, M.: The 2015 and 2016 wintertime air pollution  
520 in China: SO<sub>2</sub> emission changes derived from a WRF-Chem/EnKF coupled data  
521 assimilation system, *Atmos Chem Phys*, 19(13), 8619–8650, 2019b.



- 522 Cheng, J., Su, J., Cui, T., Li, X., Dong, X., Sun, F., Yang, Y., Tong, D., Zheng, Y., Li,  
523 Y. and others: Dominant role of emission reduction in PM<sub>2.5</sub> air quality improvement  
524 in Beijing during 2013-2017: A model-based decomposition analysis, *Atmos Chem*  
525 *Phys*, 19(9), 6125–6146, 2019.
- 526 Choi, Y.J. and Fernando, H. J. S.: Implementation of a windblown dust  
527 parameterization into MODELS-3/CMAQ: Application to episodic PM events in the  
528 US/Mexico border, *Atmos Environ*, 42(24), 6039–6046, 2008.
- 529 Clough, S. A., Shephard, M. W., Mlawer, E. J., Delamere, J. S., Iacono, M. J., Cady-  
530 Pereira, K., Boukabara, S. and Brown, P. D.: Atmospheric radiative transfer  
531 modeling: a summary of the AER codes, *J Quant Spectrosc Radiat Transf*, 91(2),  
532 233–244, 2005.
- 533 Feng, L. and Liao, W.: Legislation, plans, and policies for prevention and control of  
534 air pollution in China: achievements, challenges, and improvements, *J Clean Prod*,  
535 112, 1549–1558, 2016.
- 536 Fountoukis, C. and Nenes, A.: ISORROPIA II: a computationally efficient  
537 thermodynamic equilibrium model for K<sup>+</sup>–Ca<sup>2+</sup>–Mg<sup>2+</sup>–NH<sup>4+</sup>–Na<sup>+</sup>–SO<sub>4</sub><sup>2-</sup>–NO<sub>3</sub><sup>-</sup>–Cl<sup>-</sup>–  
538 H<sub>2</sub>O aerosols, *Atmos Chem Phys*, 7(17), 4639–4659, 2007.
- 539 Gao, M., Saide, P. E., Xin, J., Wang, Y., Liu, Z., Wang, Y., Wang, Z., Pagowski, M.,  
540 Guttikunda, S. K. and Carmichael, G. R.: Estimates of health impacts and radiative  
541 forcing in winter haze in eastern China through constraints of surface PM<sub>2.5</sub>  
542 predictions, *Environ Sci Technol*, 51(4), 2178–2185, 2017.
- 543 Geng, G., Zhang, Q., Martin, R. V, Lin, J., Huo, H., Zheng, B., Wang, S. and He, K.:  
544 Impact of spatial proxies on the representation of bottom-up emission inventories: A  
545 satellite-based analysis., *Atmos Chem Phys*, 17, 4131-4145, 2017.
- 546 Hollingsworth, A. and Lönnberg, P.: The statistical structure of short-range forecast  
547 errors as determined from radiosonde data. Part I: The wind field, *Tellus A*, 38(2),  
548 111–136, 1986.
- 549 Huang, R.-J., Zhang, Y., Bozzetti, C., Ho, K.-F., Cao, J.-J., Han, Y., Daellenbach, K.  
550 R., Slowik, J. G., Platt, S. M., Canonaco, F. and others: High secondary aerosol  
551 contribution to particulate pollution during haze events in China, *Nature*, 514(7521),  
552 218-222, 2014.
- 553 Ji, Y., Qin, X., Wang, B., Xu, J., Shen, J., Chen, J., Huang, K., Deng, C., Yan, R., Xu,  
554 K. and others: Counteractive effects of regional transport and emission control on the



- 555 formation of fine particles: a case study during the Hangzhou G20 summit, *Atmos*  
556 *Chem Phys*, 18(18), 13581–13600, 2018.
- 557 Jung, J., Souri, A. H., Wong, D. C., Lee, S., Jeon, W., Kim, J. and Choi, Y.: The  
558 Impact of the Direct Effect of Aerosols on Meteorology and Air Quality Using  
559 Aerosol Optical Depth Assimilation During the KORUS-AQ Campaign, *J Geophys*  
560 *Res Atmos*, 124(14), 8303–8319, 2019.
- 561 Kain, J. S.: The Kain-Fritsch convective parameterization: an update, *J Appl*  
562 *Meteorol*, 43(1), 170–181, 2004.
- 563 Li, B., Wang, F., Yin, H. and Li, X.: Mega events and urban air quality improvement:  
564 A temporary show?, *J Clean Prod*, 217, 116–126, 2019a.
- 565 Li, H., Wang, D., Cui, L., Gao, Y., Huo, J., Wang, X., Zhang, Z., Tan, Y., Huang, Y.,  
566 Cao, J. and others: Characteristics of atmospheric PM<sub>2.5</sub> composition during the  
567 implementation of stringent pollution control measures in shanghai for the 2016 G20  
568 summit, *Sci Total Environ*, 648, 1121–1129, 2019b.
- 569 Li, K., Jacob, D. J., Liao, H., Zhu, J., Shah, V., Shen, L., Bates, K. H., Zhang, Q. and  
570 Zhai, S.: A two-pollutant strategy for improving ozone and particulate air quality in  
571 China, *Nat Geosci*, 12(11), 906–910, 2019c.
- 572 Li, M., Zhang, Q., Kurokawa, J., Woo, J.-H., He, K., Lu, Z., Ohara, T., Song, Y.,  
573 Streets, D. G., Carmichael, G. R. and others: MIX: a mosaic Asian anthropogenic  
574 emission inventory under the international collaboration framework of the MICS-Asia  
575 and HTAP, *Atmos Chem Phys*, 17(2), 935–963, 2017a.
- 576 Li, P., Wang, L., Guo, P., Yu, S., Mehmood, K., Wang, S., Liu, W., Seinfeld, J. H.,  
577 Zhang, Y., Wong, D. C. and others: High reduction of ozone and particulate matter  
578 during the 2016 G-20 summit in Hangzhou by forced emission controls of industry  
579 and traffic, *Environ Chem Lett*, 15(4), 709–715, 2017b.
- 580 Li, X., Choi, Y., Czader, B., Roy, A., Kim, H., Lefer, B. and Pan, S.: The impact of  
581 observation nudging on simulated meteorology and ozone concentrations during  
582 DISCOVER-AQ 2013 Texas campaign, *Atmos Chem Phys*, 16(5), 3127–3144, 2016.
- 583 Liu, H., Liu, C., Xie, Z., Li, Y., Huang, X., Wang, S., Xu, J. and Xie, P.: A paradox  
584 for air pollution controlling in China revealed by “APEC Blue” and “Parade Blue,”  
585 *Sci Rep*, 6(1), 1–13, 2016.
- 586 Liu, Z., Guan, D., Wei, W., Davis, S. J., Ciais, P., Bai, J., Peng, S., Zhang, Q.,  
587 Hubacek, K., Marland, G. and others: Reduced carbon emission estimates from fossil  
588 fuel combustion and cement production in China, *Nature*, 524(7565), 335–338, 2015.



- 589 Ma, C., Wang, T., Mizzi, A. P., Anderson, J. L., Zhuang, B., Xie, M. and Wu, R.:  
590 Multi-constituent data assimilation with WRF-Chem/DART: Potential for adjusting  
591 anthropogenic emissions and improving air quality forecasts over eastern China, *J*  
592 *Geophys Res Atmos*, 2019.
- 593 Ma, Z., Hu, X., Huang, L., Bi, J. and Liu, Y.: Estimating ground-level PM<sub>2.5</sub> in China  
594 using satellite remote sensing, *Environ Sci Technol*, 48(13), 7436–7444, 2014.
- 595 Ma, Z., Hu, X., Sayer, A. M., Levy, R., Zhang, Q., Xue, Y., Tong, S., Bi, J., Huang,  
596 L. and Liu, Y.: Satellite-based spatiotemporal trends in PM<sub>2.5</sub> concentrations: China,  
597 2004–2013, *Environ Health Perspect*, 124(2), 184–192, 2015.
- 598 Morrison, H. and Gettelman, A.: A new two-moment bulk stratiform cloud  
599 microphysics scheme in the Community Atmosphere Model, version 3 (CAM3). Part  
600 I: Description and numerical tests, *J Clim*, 21(15), 3642–3659, 2008.
- 601 Mu, Q. and Liao, H.: Simulation of the interannual variations of aerosols in China:  
602 role of variations in meteorological parameters, *Atmos Chem Phys*, 14, 11177–11219,  
603 2014.
- 604 Pleim, J. E.: A combined local and nonlocal closure model for the atmospheric  
605 boundary layer. Part I: Model description and testing, *J Appl Meteorol Climatol*,  
606 46(9), 1383–1395, 2007a.
- 607 Pleim, J. E.: A combined local and nonlocal closure model for the atmospheric  
608 boundary layer. Part II: Application and evaluation in a mesoscale meteorological  
609 model, *J Appl Meteorol Climatol*, 46(9), 1396–1409, 2007b.
- 610 Rutherford, I. D.: Data assimilation by statistical interpolation of forecast error fields,  
611 *J Atmos Sci*, 29(5), 809–815, 1972.
- 612 Seinfeld, J. H. and Pandis, S. N.: *Atmospheric chemistry and physics: from air*  
613 *pollution to climate change*, John Wiley & Sons., 2016.
- 614 Sheehan, P., Cheng, E., English, A. and Sun, F.: China's response to the air pollution  
615 shock, *Nat Clim Chang*, 4(5), 306–309, 2014.
- 616 Shi, H., Wang, Y., Chen, J. and Huisingh, D.: Preventing smog crises in China and  
617 globally, *J Clean Prod*, 112, 1261–1271, 2016.
- 618 Shu, L., Wang, T., Han, H., Xie, M., Chen, P., Li, M. and Wu, H.: Summertime ozone  
619 pollution in the Yangtze River Delta of eastern China during 2013--2017: Synoptic  
620 impacts and source apportionment, *Environ Pollut*, 113631, 2019.



- 621 Sun, Y., Wang, Z., Wild, O., Xu, W., Chen, C., Fu, P., Du, W., Zhou, L., Zhang, Q.,  
622 Han, T. and others: “APEC blue”: secondary aerosol reductions from emission  
623 controls in Beijing, *Sci Rep*, 6, 20668, 2016.
- 624 Tai, A. P. K., Mickley, L. J. and Jacob, D. J.: Impact of 2000–2050 climate change on  
625 fine particulate matter (PM<sub>2.5</sub>) air quality inferred from a multi-model analysis of  
626 meteorological modes, *Atmos Chem Phys*, 12, 11329–11337, 2012.
- 627 Wang, J., Zhao, B., Wang, S., Yang, F., Xing, J., Morawska, L., Ding, A., Kulmala,  
628 M., Kerminen, V.-M., Kujansuu, J. and others: Particulate matter pollution over China  
629 and the effects of control policies, *Sci Total Environ*, 584, 426–447, 2017.
- 630 Wang, P., Guo, H., Hu, J., Kota, S. H., Ying, Q. and Zhang, H.: Responses of PM<sub>2.5</sub>  
631 and O<sub>3</sub> concentrations to changes of meteorology and emissions in China, *Sci Total*  
632 *Environ*, 662, 297–306, 2019.
- 633 Wong, D. C., Pleim, J., Mathur, R., Binkowski, F., Otte, T., Gilliam, R., Pouliot, G.,  
634 Xiu, A., Young, J. O. and Kang, D.: WRF-CMAQ two-way coupled system with  
635 aerosol feedback: software development and preliminary results, *Geosci Model Dev*,  
636 5(2), 299–312, 2012.
- 637 Xie, H., Wang, L., Ling, X., Miao, Y., Shen, X., Wang, M. and Xin, Y.: China air  
638 quality management assessment report (2016), 2015.
- 639 Xiu, A. and Pleim, J. E.: Development of a land surface model. Part I: Application in  
640 a mesoscale meteorological model, *J Appl Meteorol*, 40(2), 192–209, 2001.
- 641 Xue, T., Zheng, Y., Tong, D., Zheng, B., Li, X., Zhu, T. and Zhang, Q.:  
642 Spatiotemporal continuous estimates of PM<sub>2.5</sub> concentrations in China, 2000–2016: A  
643 machine learning method with inputs from satellites, chemical transport model, and  
644 ground observations, *Environ Int*, 123, 345–357, 2019.
- 645 Yan, B., Liu, S., Zhao, B., Li, X., Fu, Q. and Jiang, G.: China’s fight for clean air and  
646 human health, 2018.
- 647 Yang, W., Yuan, G. and Han, J.: Is China’s air pollution control policy effective?  
648 Evidence from Yangtze River Delta cities, *J Clean Prod*, 220, 110–133, 2019.
- 649 Yarwood, G., Rao, S., Yocke, M. and Whitten, G. Z.: Updates to the carbon bond  
650 chemical mechanism: CB05, Final Rep to US EPA, RT-0400675, 8, 2005.
- 651 Yu, S., Li, P., Wang, L., Wu, Y., Wang, S., Liu, K., Zhu, T., Zhang, Y., Hu, M., Zeng,  
652 L. and others: Mitigation of severe urban haze pollution by a precision air pollution  
653 control approach, *Sci. Rep.*, 8(1), 8151, 2018.



654 Yu, S., Eder, B., Dennis, R., Chu, S.-H. and Schwartz, S. E.: New unbiased  
655 symmetric metrics for evaluation of air quality models, *Atmos. Sci. Lett.*, 7(1), 26–34,  
656 2006.

657 Yu, S., Mathur, R., Pleim, J., Wong, D., Gilliam, R., Alapaty, K., Zhao, C. and Liu,  
658 X.: Aerosol indirect effect on the grid-scale clouds in the two-way coupled WRF-  
659 CMAQ: model description, development, evaluation and regional analysis, *Atmos*  
660 *Chem Phys*, 14, 11247–11285, 2014.

661 Zhang, L., Shao, J., Lu, X., Zhao, Y., Hu, Y., Henze, D. K., Liao, H., Gong, S. and  
662 Zhang, Q.: Sources and processes affecting fine particulate matter pollution over  
663 North China: an adjoint analysis of the Beijing APEC period, *Environ Sci Technol*,  
664 50(16), 8731–8740, 2016.

665 Zhang, Q., He, K. and Huo, H.: Policy: cleaning China’s air, *Nature*, 484(7393), 161,  
666 2012.

667 Zhang, Q., Zheng, Y., Tong, D., Shao, M., Wang, S., Zhang, Y., Xu, X., Wang, J.,  
668 He, H., Liu, W. and others: Drivers of improved PM<sub>2.5</sub> air quality in China from 2013  
669 to 2017, *Proc Natl Acad Sci*, 2019.

670 Zhang, R., Wang, G., Guo, S., Zamora, M. L., Ying, Q., Lin, Y., Wang, W., Hu, M.  
671 and Wang, Y.: Formation of urban fine particulate matter, *Chem Rev*, 115(10), 3803–  
672 3855, 2015.

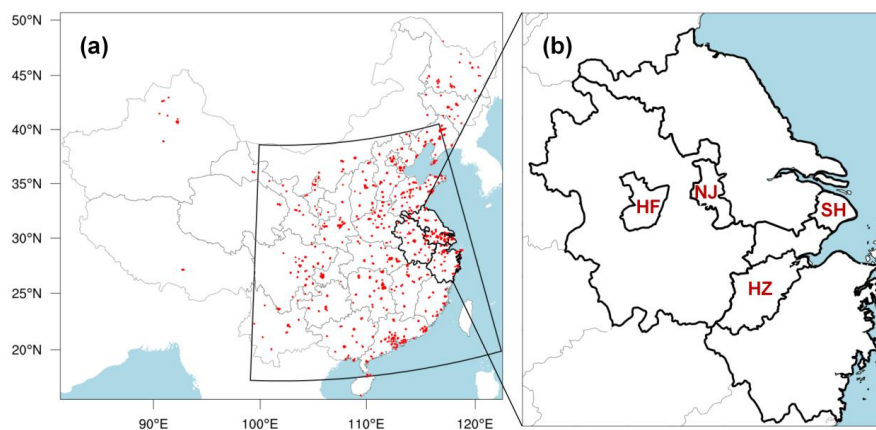
673 Zhang, Y.-L. and Cao, F.: Fine particulate matter (PM<sub>2.5</sub>) in China at a city level, *Sci*  
674 *Rep*, 5, 14884, 2015.

675 Zheng, B., Tong, D., Li, M., Liu, F., Hong, C., Geng, G., Li, H., Li, X., Peng, L., Qi,  
676 J. and others: Trends in China’s anthropogenic emissions since 2010 as the  
677 consequence of clean air actions, *Atmos Chem Phys*, 18(19), 14095–14111, 2018.

678  
679  
680  
681  
682  
683  
684  
685  
686  
687



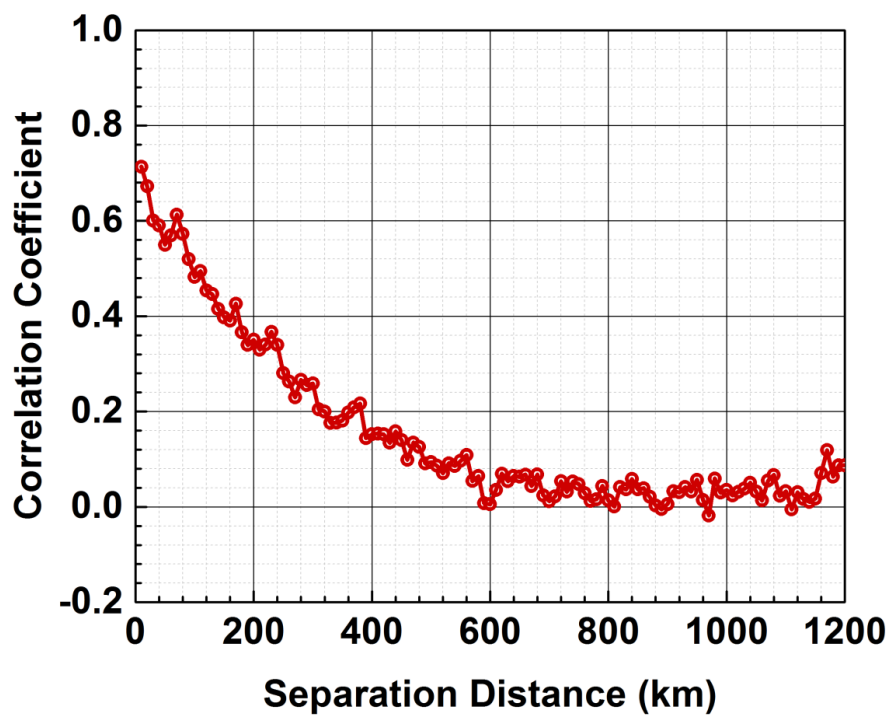
688  
689



690  
691

692 **Figure 1. (a) The model domain. Red dots denote the ground-level PM<sub>2.5</sub>**  
693 **measurements, which, within the fan-shaped quadrilateral, are used to constrain**  
694 **the model predictions. (b) Black lines outline the boundaries of the Yangtze River**  
695 **Delta (YRD), as well as four major cities considered (i.e., SH: Shanghai; HZ:**  
696 **Hangzhou; NJ: Nanjing; HF: Hefei).**

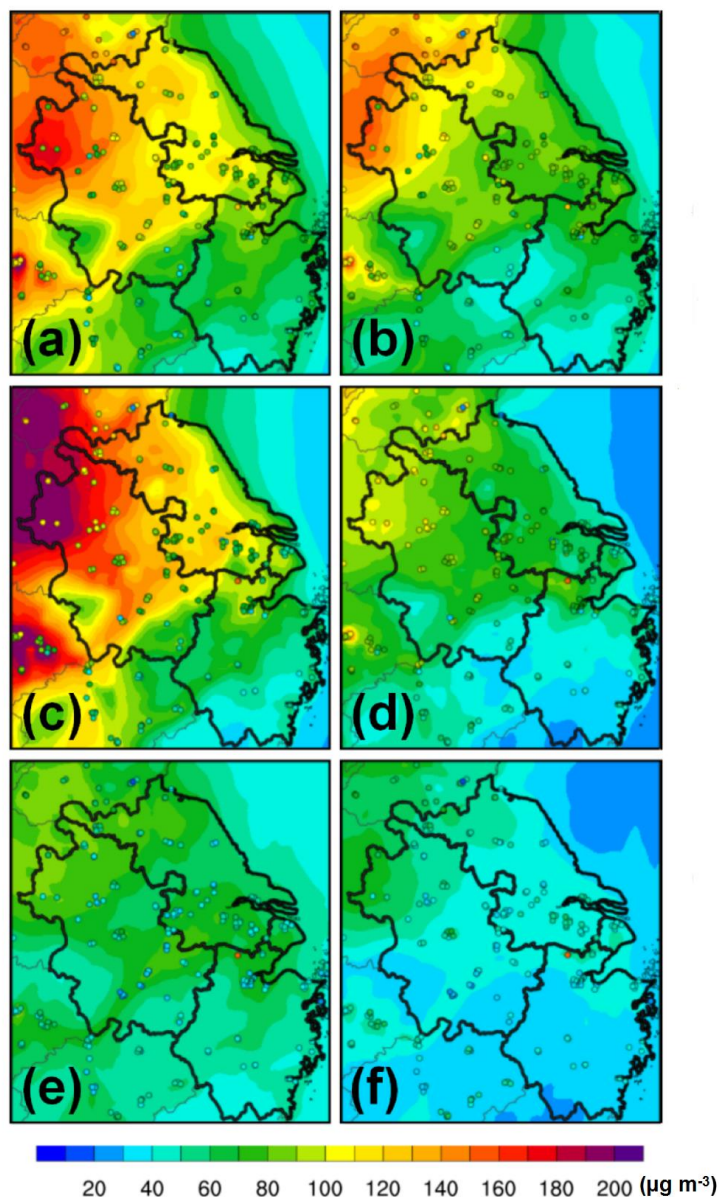
697  
698  
699  
700  
701  
702  
703  
704  
705



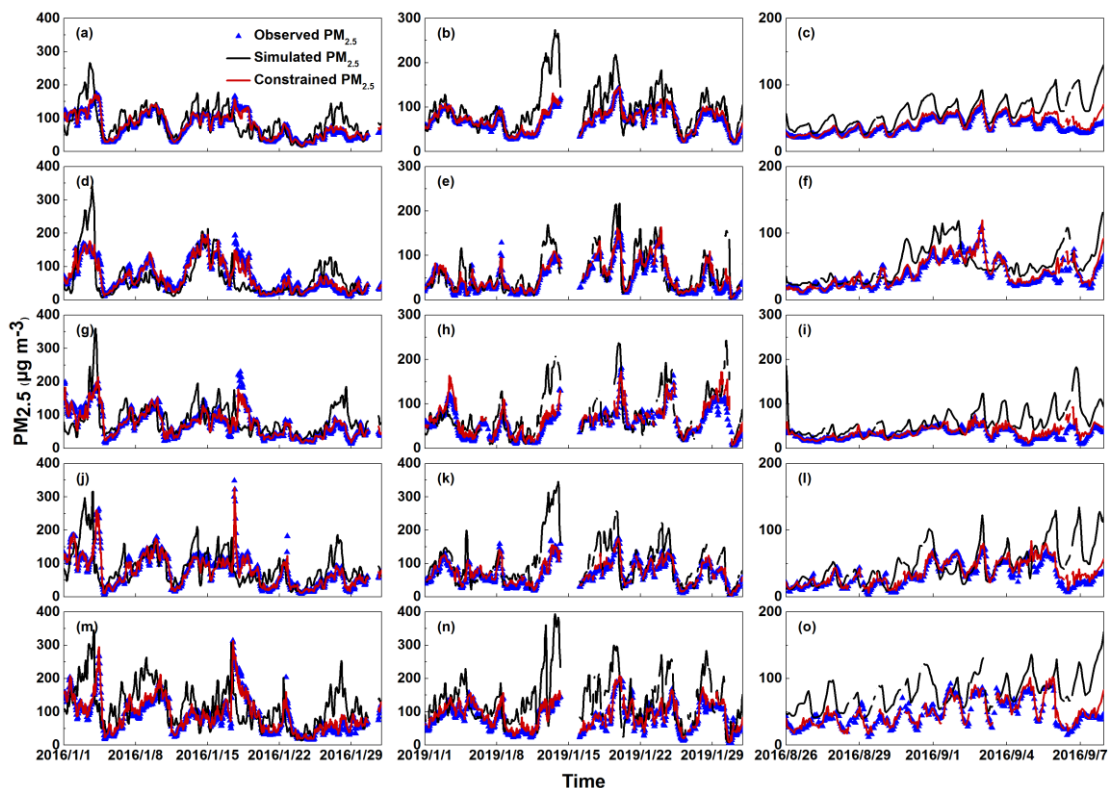
706  
707

708 **Figure 2.** Correlation coefficients (averaged over 10 km) as a function of the  
709 separation distances between two surface-level monitoring stations using the  
710 **Hollingsworth-Lönberg method.**

711



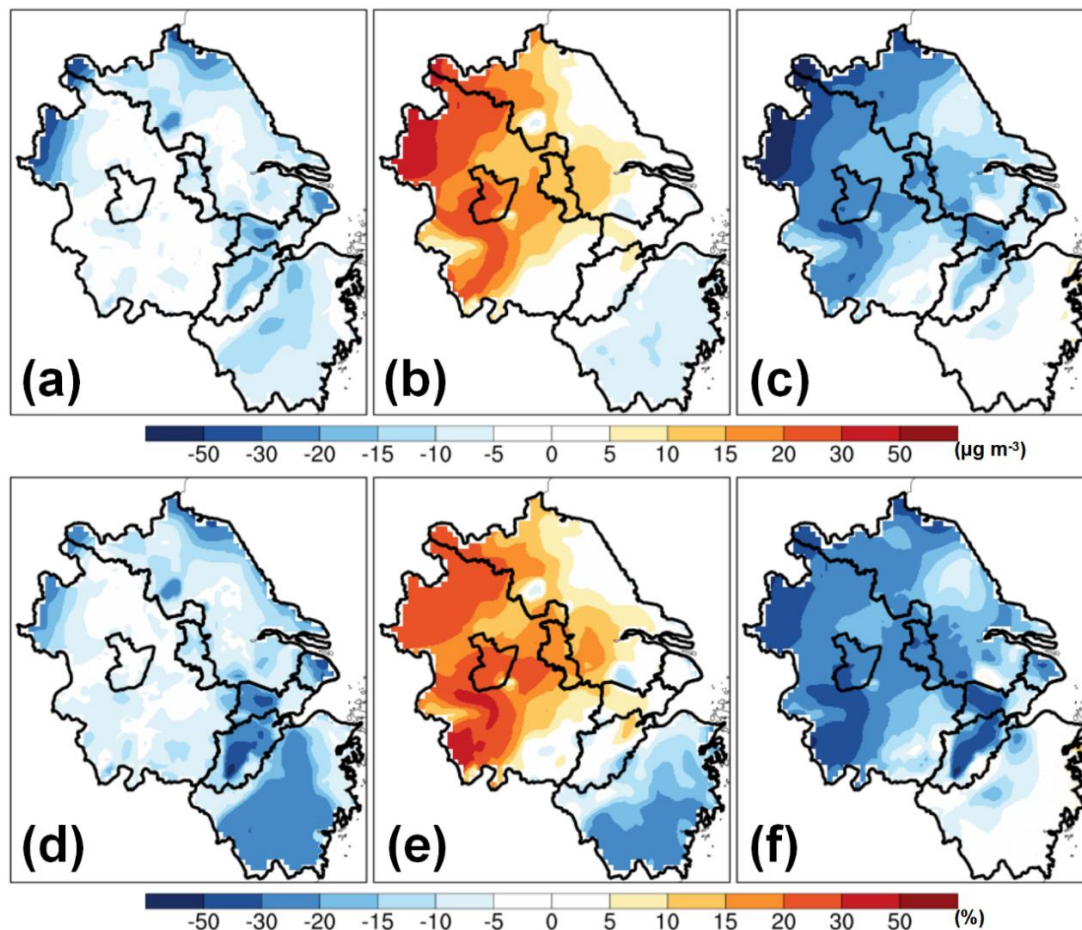
712  
713 **Figure 3.** Spatial comparisons of hourly-averaged concentrations of simulated and  
714 **constrained PM<sub>2.5</sub> with surface observations across the YRD for January 2016 (top**  
715 **panel), January 2019 (middle panel), and the G20 summit (bottom panel): (a)**  
716 **NO\_2016; (b) DA\_2016; (c) NO\_2019; (d) DA\_2019; (e) NO\_G20; (f) DA\_G20.**  
717 **Circles denote ground measurement sites.**



718

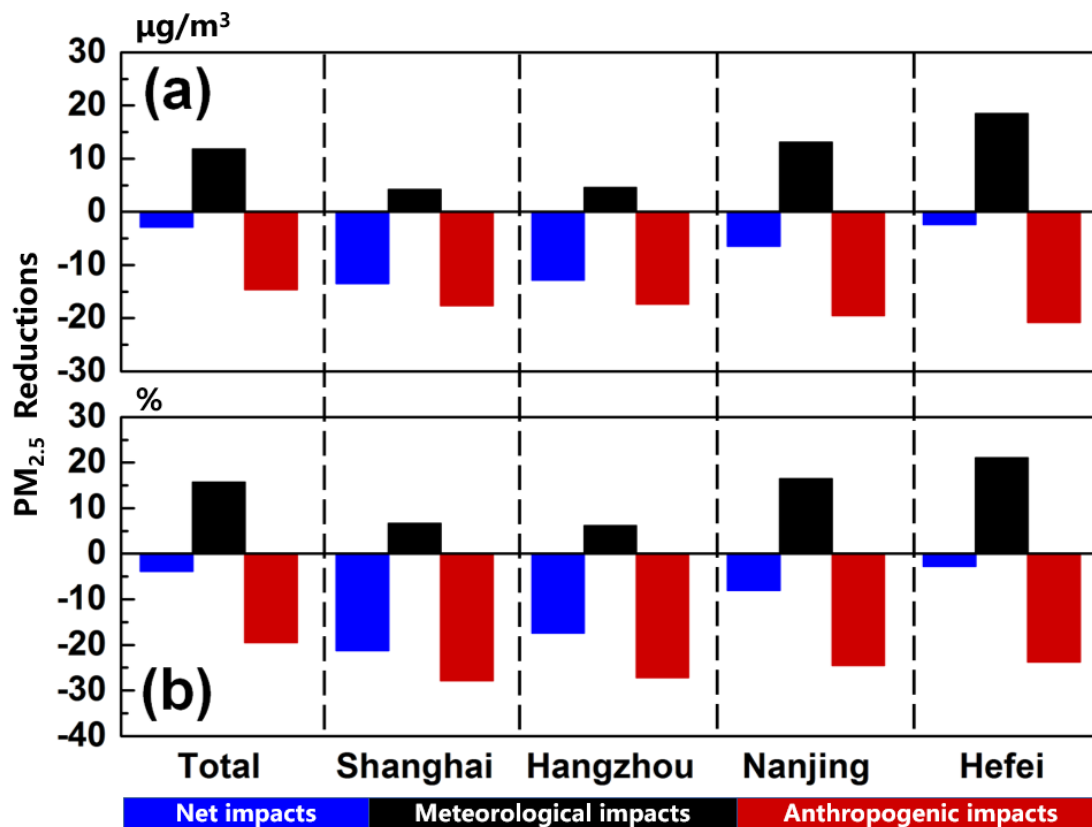
719

720 **Figure 4. Time series of the comparisons between hourly observed, simulated, and**  
721 **constrained PM<sub>2.5</sub> concentrations for January 2016 (left column), January 2019**  
722 **(middle column), and the G20 summit (right column) over (a – c) the whole domain**  
723 **as well as in four representative cities, which are as follows: (d - f) Shanghai, (g -**  
724 **i) Hangzhou, (j - l) Nanjing, and (m - o) Hefei. The black circles, black lines, and**  
725 **red lines denote the hourly observed, simulated, and constrained PM<sub>2.5</sub>**  
726 **concentrations, respectively.**



727  
728

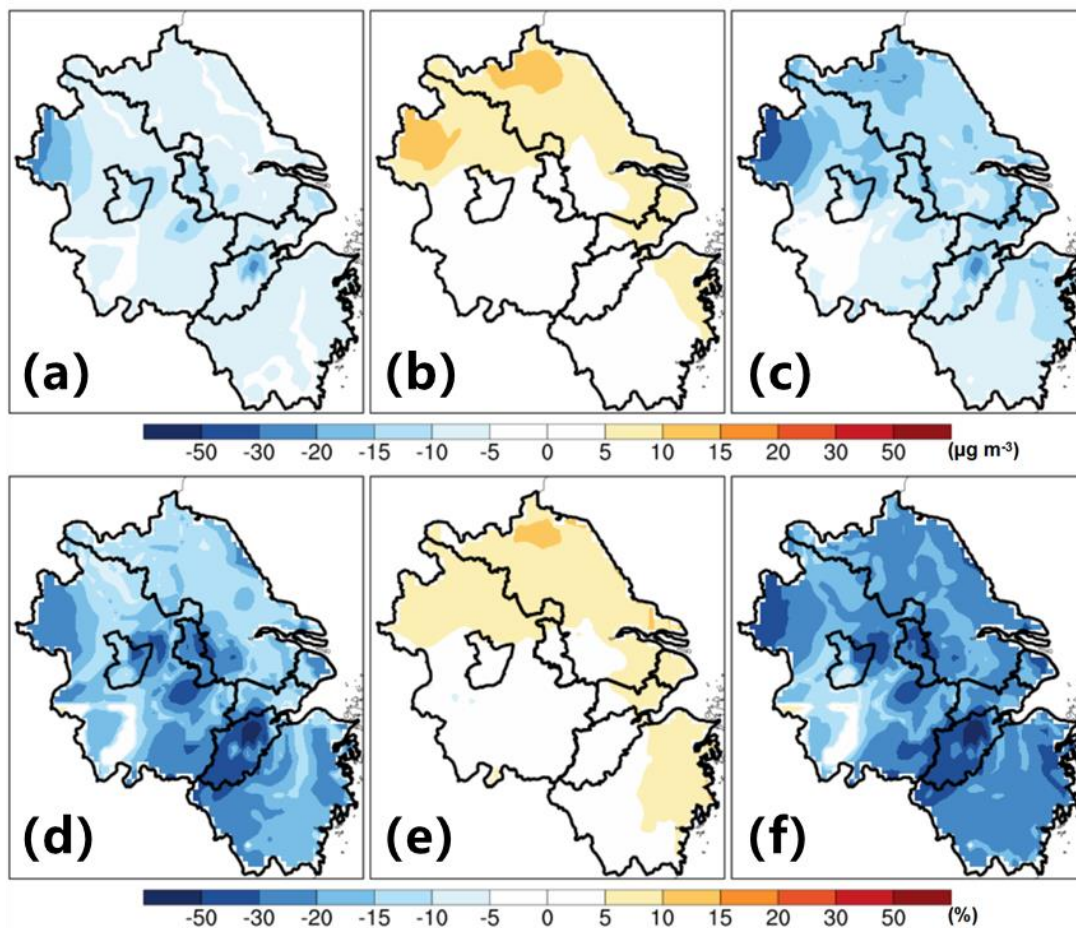
729 **Figure 5.** The impacts of anthropogenic emission controls and meteorological  
730 variations on spatial  $\text{PM}_{2.5}$  concentrations in January from 2016 to 2019. (a, d)  
731 Their net impacts. (b, e) meteorological impacts. (c, f) the impacts of  
732 anthropogenic emission controls. The top and bottom panels refer to the changes  
733 in absolute values and relative percentages, respectively.



734

735

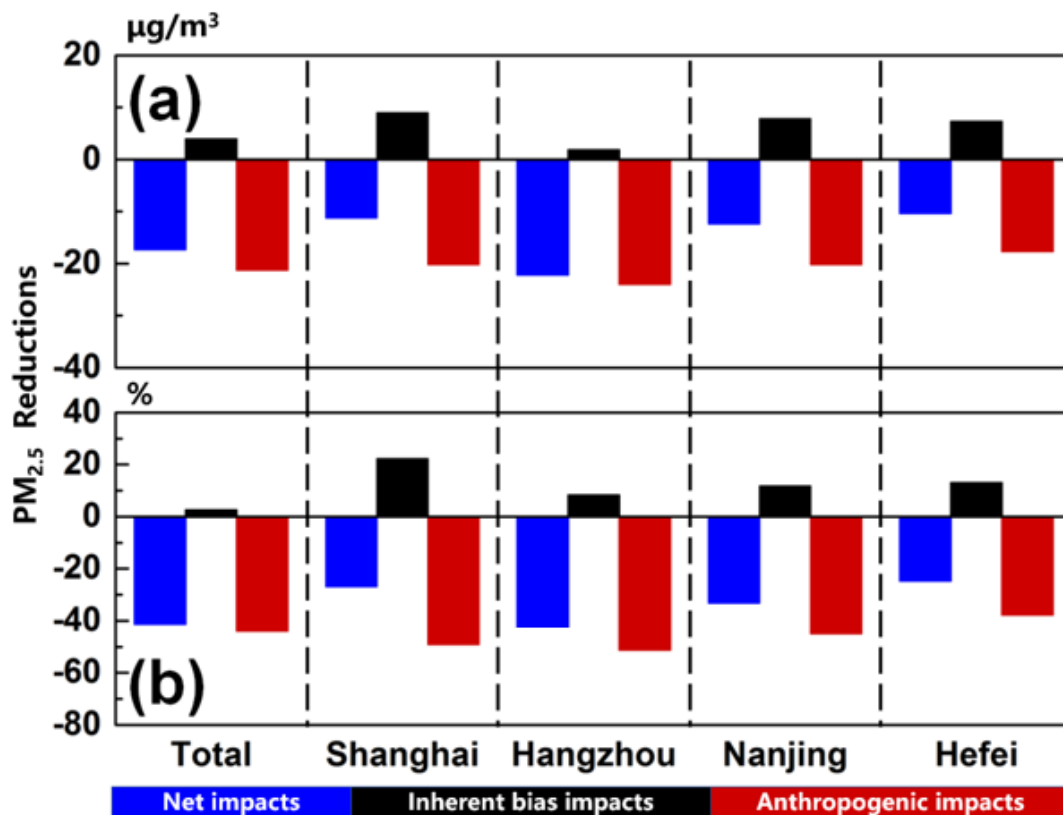
736 **Figure 6.** The impacts of anthropogenic emission controls and meteorological  
737 variations on PM<sub>2.5</sub> concentrations in January from 2016 to 2019 over the whole  
738 domain as well as in four representative cities (i.e., Shanghai, Hangzhou, Nanjing,  
739 and Hefei). The top and bottom panels refer to the changes in absolute values and  
740 relative percentages, respectively.



741

742

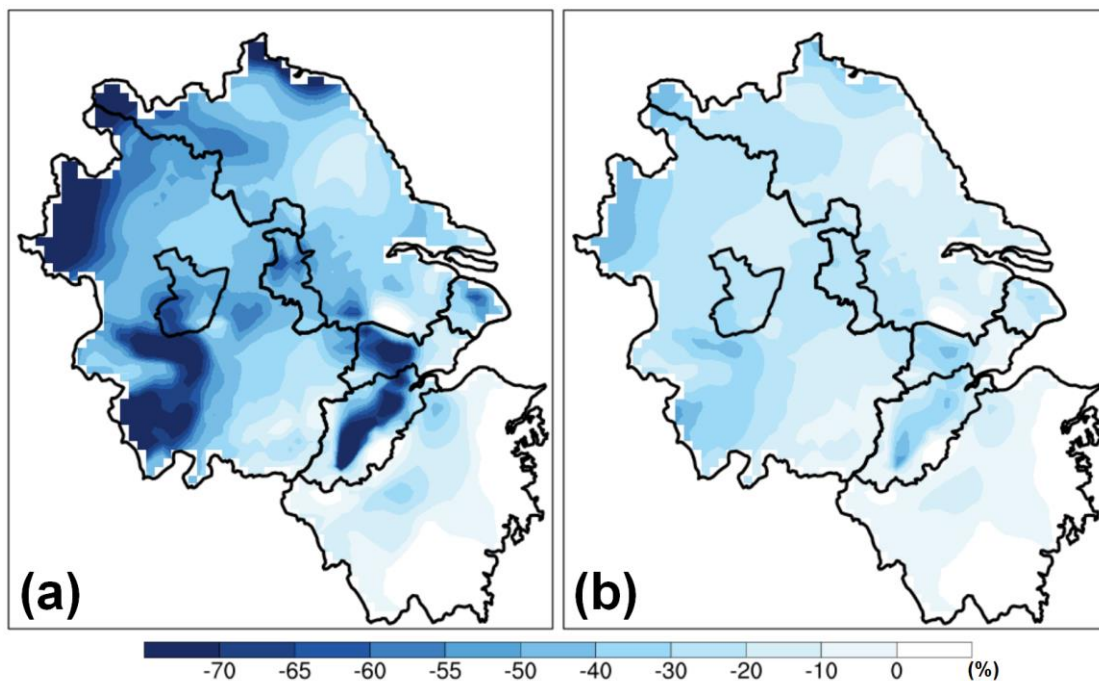
743 **Figure 7. The impacts of anthropogenic emission controls and inherent biases on**  
744 **spatial PM<sub>2.5</sub> concentrations during the G20 summit. (a, d) Their net impacts. (b,**  
745 **e) the impacts of inherent biases. (c, f) the impacts of anthropogenic emission**  
746 **controls. The top and bottom panels refer to the changes in absolute values and**  
747 **relative percentages, respectively. Inherent biases are mainly due to the prior**  
748 **anthropogenic emissions.**



749

750

751 **Figure 8. The impacts of anthropogenic emission controls and inherent biases on**  
752 **PM<sub>2.5</sub> concentrations during the G20 summit over the whole domain as well as in**  
753 **four representative cities (i.e., Shanghai, Hangzhou, Nanjing, and Hefei). The top**  
754 **and bottom panels refer to the changes in absolute values and relative percentages,**  
755 **respectively. Inherent biases are mainly due to the prior anthropogenic emissions.**



756

757

758 **Figure 9. (a) Spatial distributions of the PM<sub>2.5</sub> mitigation potential across the YRD**  
759 **and (b) their differences with the impacts of long-term emission control strategies**  
760 **from 2016 to 2019 (Fig. 5f). Both spatial patterns of long-term emission control**  
761 **strategy impacts (Fig. 5f) and the localized PM<sub>2.5</sub> mitigation potential in the main**  
762 **urban areas of Hangzhou (Fig. S10), with the proportion calculator, result in Fig.**  
763 **9a.**

764

765

766

767

768

769



770 **Table 1. The experiments to isolate the effects of anthropogenic emission controls**  
 771 **due to the long-term and emergency emission control strategies.**

772

Experiments	Time Periods	Constrained Meteorology	Constrained Observations	Comparisons and Purposes
DA_2016	January 2016	Yes	Yes	The net effects of major driving factors (i.e., anthropogenic emission controls and meteorological variations) from 2016 to 2019.
DA_2019	January 2019	Yes	Yes	
NO_2016	January 2016	Yes	No	The effects of meteorological variations from 2016 to 2019.
NO_2019	January 2019	Yes	No	
DA_G20		Yes	Yes	The net effects of major driving factors (i.e., anthropogenic emission controls and the uncertainties in the priori anthropogenic emissions) during the G20 summit.
NO_G20	August 26 to September 7, 2016	Yes	No	
DA_CON_G20	August 11 to August 23 and September 18	Yes	Yes	The effects of the uncertainties in the priori anthropogenic emissions.
NO_CON_G20	to September 30, 2016	Yes	No	

773